Journal of Power Sources 195 (2010) 3359–3364

Contents lists available at ScienceDirect

Journal of Power Sources

journal homepage: www.elsevier.com/locate/jpowsour

Electrode performance and analysis of reversible solid oxide fuel cells with proton conducting electrolyte of $BaCe_{0.5}Zr_{0.3}Y_{0.2}O_{3-\delta}$

Fei He, Duo Song, Ranran Peng*, Guangyao Meng, Shangfeng Yang

CAS Key Laboratory of Materials for Energy Conversion, Department of Materials Science and Engineering, University of Science and Technology of China, JinZhai Road 96, Hefei, 230026 Anhui, China

ARTICLE INFO

Article history:
Received 20 November 2009
Received in revised form
17 December 2009
Accepted 17 December 2009
Available online 29 December 2009

Keywords:
Solid oxide fuel cells (SOFCs)
Solid oxide electrolysis cells (SOECs)
Proton conducting electrolytes
Electrode performance
AC impedance spectra

ABSTRACT

Reversible solid oxide fuel cells (R-SOFCs) are regarded as a promising solution to the discontinuity in electric energy, since they can generate electric powder as solid oxide fuel cells (SOFCs) at the time of electricity shortage, and store the electrical power as solid oxide electrolysis cells (SOECs) at the time of electricity over-plus. In this work, R-SOFCs with thin proton conducting electrolyte films of $BaCe_{0.5}Zr_{0.3}Y_{0.2}O_{3-\delta}$ were fabricated and their electro-performance was characterized with various reacting atmospheres. At 700 °C, the charging current (in SOFC mode) is 251 mA cm^{-2} at 0.7 V, and the electrolysis current densities (in SOEC mode) reaches −830 mA cm^{-2} at 1.5 V with 50% H_2O–air and H_2 as reacting gases, respectively. Their electrode performance was investigated by impedance spectra in discharging mode (SOFC mode), electrolysis mode (SOEC mode) and open circuit mode (OCV mode). The results show that impedance spectra have different shapes in all the three modes, implying different rate-limiting steps. In SOFC mode, the high frequency resistance (R_H) is 0.07 Ωcm^2 and low frequency resistances (R_L) are 0.37 Ωcm^2. While in SOEC mode, R_H is 0.15 Ωcm^2, twice of that in SOFC mode, and R_L is only 0.07 Ωcm^2, about 19% of that in SOFC mode. Moreover, the spectra under OCV conditions seems like a combination of those in SOEC mode and SOFC mode, since that R_H in OCV mode is about 0.13 Ωcm^2, close to R_H in SOEC mode, while R_L in OCV mode is 0.39 Ωcm^2, close to R_L in SOFC mode. The elementary steps for SOEC with proton conducting electrolyte were proposed to account for this phenomenon.

1. Introduction

Solid oxide fuel cells (SOFCs) have drawn much attention as a clean and effective power generation system, which efficiently generate electrical powder with the consumption of H_2 and O_2 [1], as shown in Eq. (1). As the reverse reaction of Eq. (1), water can be electrolyzed to H_2 and O_2, and the reversible operation of SOFCs was called as solid oxide electrolysis cells (SOECs), which has become increasingly investigated as a green and high-efficiency technology for large-scale hydrogen production [2–8]. Since the cells can work as SOFCs at the time of electricity shortage to generate electrical powder, and as SOECs at the time of electricity over-plus to store the electrical power by the production of electrochemical substances (H_2), these solid cells are also called as "reversible solid oxide fuel cells (R-SOFCs)" [9,10]. R-SOFCs are deemed as a promising solution to the discontinuity in renewable electric energy, which might be generated by solar energy, wind energy, and tidal energy.

$$H_2 + \tfrac{1}{2}O_2 \leftrightarrow H_2O \quad (1)$$

Some achievements have been made in the research of R-SOFCs or SOEC with oxygen-ion conducting electrolytes [2–8]. Liang et al. precipitated LSM on submicron-sized YSZ particles by glycine-nitrate process (GNP) as oxygen electrode, and the electrolysis current densities improved to 0.520 A cm^{-2} at 900 °C with 12-μm-thick yttrium stabilized zirconia (YSZ) as electrolyte [4]. Laguna-Bercero et al. [5] used 10% Sc_2O_3–1% CeO_2–ZrO_2(SCZ) as electrolyte, and the electrolysis current density was 420 mA cm^{-2} at 1.5 V measured at 700 °C with 80% steam concentration introduced to hydrogen electrode. Schiller et al. [11] deposited subsequently a $La_{0.7}Sr_{0.15}Ca_{0.15}CrO_3$ diffusion barrier layer, a 50-μm-thick Ni/YSZ hydrogen electrode, a 40-μm-thick YSZ electrolyte and a 30-μm-thick LSCF oxygen electrode on 1-mm-thick porous metal sheet of ferritic steel (IT11) substrate by plasma spray technology, and the electrolysis current density of cells reached 1.0 A cm^{-2} at 1.4 V measured at 800 °C. Yet Ni et al. [12] studied the electrochemical performance of R-SOFCs with oxygen-ion conducting electrolyte (R-SOECs-O), and found that the cathode-supported configurations (in SOFC mode) are more favorable for electrolysis due to the smaller concentration polarization, which was quite opposite to the promising SOFC configuration. While his simulation performance of R-SOFC with proton conducting electrolyte (R-SOFCs-H) indicated that the anode-supported configuration (in SOFC mode) was

* Corresponding author. Tel.: +86 551 3600594; fax: +86 551 3607475.
E-mail address: pengrr@ustc.edu.cn (R. Peng).

0378-7753/$ – see front matter © 2009 Elsevier B.V. All rights reserved.
doi:10.1016/j.jpowsour.2009.12.079

favorable to achieve high energy conversion efficiency in both SOFC and SOEC modes. This is because that water generated (injected) in SOFC cathode for R-SOFCs-H, which acquires thin cathode film to reduce the concentration polarization [13]. Besides the configuration advantages, R-SOFCs-H has other benefits, such as: (1) no need of H_2 separation, since H_2O is introduced into the oxygen electrode side and that pure H_2 can be obtained with H_2 as gas carrier; (2) lower activation energy for proton conduction suitable for application in intermediate temperature R-SOFCs.

In 1981, Iwahara et al. [14] firstly applied $SrCeO_3$ as the proton conducting electrolyte in steam electrolysis to produce hydrogen gas. Since then, novel materials with improved conductivity, such as $SrZr_{0.9}Yb_{0.1}O_{3-\alpha}$ [15], $BaCe_{0.9}Sr_{0.1}O_{3-\delta}$ [16], $SrZr_{0.9}Y_{0.1}O_{3-\delta}$ [17], have been investigated as the electrolyte in steam electrolysis and their electrolysis current densities were about 40 mA cm^{-2} at 1.5 V. Till now, most investigations on SOEC focus on exploring electrolyte materials, and few systematic investigations of the electrode reactions have been reported. In this work, the electrode performance of R-SOFCs was studied using $BaCe_{0.5}Zr_{0.3}Y_{0.2}O_{3-\delta}$ proton conducting electrolytes. And the characteristics of the electrode behavior under various steam partial pressures were investigated by impedance spectra in both SOFC mode and SOEC mode, which is further compared with those under open circuit conditions.

2. Experimental

2.1. Preparation of $BaCe_{0.5}Zr_{0.3}Y_{0.2}O_{3-\delta}$ powders

$BaCe_{0.5}Zr_{0.3}Y_{0.2}O_{3-\delta}$ (BCZY) powders were synthesized by citric method. A proper amount of EDTA was dissolved in deionized water with ammonia added to adjust the pH value to 6. Stoichiometric amount of Ba^{2+}, Ce^{3+}, Zr^{4+}, Y^{3+} nitrates solution was mixed with the EDTA solution, and then citric acid was added as complex to form a precursor solution. The molar ratio of Ba^{2+}, EDTA and citric acid was set as 1: 2.4: 2.4. The as-prepared precursor solution was stirred at 80 °C for 3–4 h and then heated on a hot plate. As the evaporation proceeded, the solution became viscous gel, and turned into a foamy black sponge, which ignited and resulted in black powders. The powders were sintered at 1100 °C for 2 h to remove the carbon residues and to form perovskite BCZY. $Sm_{0.5}Sr_{0.5}CoO_{3-\delta}$ (SSC) and NiO powders were synthesized by GNP, as described elsewhere [18,19].

2.2. Fabrication of reversible solid oxide fuel cells (R-SOFCs)

The electrodes of R-SOFC were described as hydrogen electrode and oxygen electrode, respectively, to avoid misunderstanding of the anodes and cathodes in SOFC mode or SOEC mode. NiO and BCZY powders were mixed in a weight ratio of 65:35 as hydrogen electrode. Bi-layers of the anode substrate and BCZY electrolyte of about 15 mm in diameter were fabricated by a dry-pressing method. The thickness of electrolyte was about 20 μm after the bi-layers were co-sintered at 1400 °C for 5 h in air. SSC and BCZY powders were mixed as oxygen electrode powders with the weight ratio of 70:30. The oxygen electrode layers of about 40 μm in thickness and 6 mm in diameter were formed by screen-printing process with ethocel and abietyl alcohol as binder, and then fired at 1100 °C for 2 h in air to form single reversible cells. Ag paste was applied onto the oxygen electrode surface as the current collector. Accordingly, the R-SOFCs with structure of Ni-BCZY || $BaCe_{0.5}Zr_{0.3}Y_{0.2}O_{3-\delta}$ (BCZY) || SSC–BCZY were fabricated.

2.3. Characterizations of the R-SOFCs

The reversible single cells were tested with a home-developed-cell-testing system. Air/H_2O mixture and H_2 were introduced into oxygen electrode and hydrogen electrode as testing gases, respectively. The steam partial pressures in air/H_2O were set in the range of 20–70% by controlling by the temperature of gas bubble, where dry air flowed at a constant flow rate of 100 ml min^{-1}. The gas flow of H_2 is 70 ml min^{-1}. The impedance spectra of single cells were measured under open circuit conditions, SOEC mode (1.3 V), and SOFC mode (0.7 V), respectively, using an electrochemical workstation (IM6e, Zahner). Curve fittings were performed using the Z-view software. The cells were characterized in both fuel-cell and electrolysis-cell operation by *I–V* measurements using an electrochemical workstation (IM6e, Zahner) tested at 600–700 °C.

3. Results and discussion

3.1. Electrochemical performance of the Reversible SOFCs

The electrochemical performances of R-SOFCs were investigated in both SOFC mode and SOEC mode, as shown in Fig. 1, in which the positive current density refers to fuel-cell operation and the negative current density refers to electrolysis-cell operation. With 50%air–50%H_2O and H_2 introduced into air electrode and hydrogen electrode, respectively, the open circuit voltages (OCVs) of cells are 0.97, 0.96, 0.95 V at 600, 650 and 700 °C, respectively. These OCVs are very close to the theoretical electromotive force (EMF) calculated by Nernst equation, which are 1.04, 1.03, 1.01 V at 600, 650 and 700 °C, respectively, indicating that the electrolyte film are very dense.

In SOFC mode (the right part of Fig. 1), H_2 react with O_2 to generate electrical power, and the charging current densities are 70, 163, and 251 mA cm^{-2} at 0.7 V at 600, 650 and 700 °C, respectively. The maxima power density reached about 69, 140, 234 mW cm^{-2} at 0.48 V measured at 600, 650 and 700 °C, respectively. The area specific resistances (ASRs) of the cell in SOFC mode can be calculated by the slope of the *I–V* curves with the section of potential below the OCV. At 600, 650 and 700 °C, the ASRs of the cell are 2.28, 1.22, 0.82 Ωcm^2, respectively. On the other hand, the performance of cells in the SOEC mode also increases with temperature (see the left panel of Fig. 1), and the electrolysis current densities at cell voltage of 1.5 V are −326, −565, −830 mA cm^{-2} at 600, 650 and 700 °C, respectively. The ASRs in SOEC mode at 600, 650 and 700 °C are 1.48, 0.78, 0.51 Ωcm^2, respectively, which are obviously lower than that obtained in SOFC mode.

The impedance spectra of the cells under open circuit conditions are investigated and the spectra obtained under different temperatures are shown in Fig. 2. Obviously the cell resistances

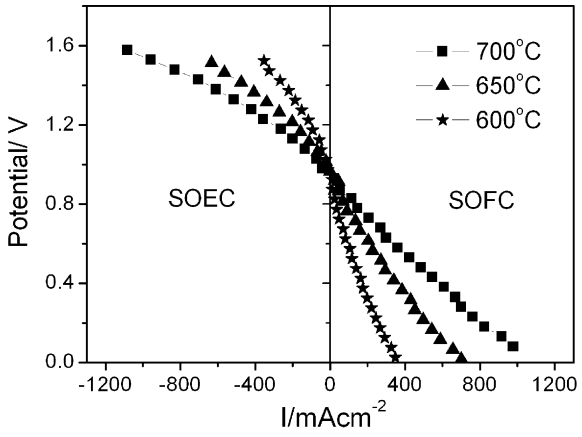

Fig. 1. *I–V* curves of reversible solid oxide fuel cells (R-SOFCs) measured at various temperatures. H_2 and 50%H_2O–50%air are used as the reacting gases in hydrogen electrode and oxygen electrode, respectively.

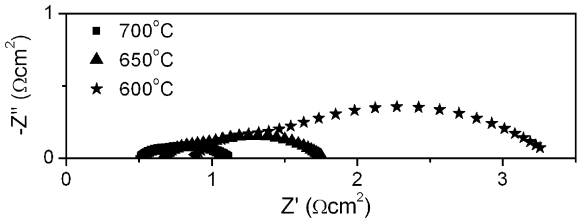

Fig. 2. Impedance spectra of R-SOFCs measured at various temperatures with 50%H_2O–50%air and H_2 as reacting gases.

decrease with the increase of temperature. The bulk resistances of cell are 0.89, 0.67 and 0.53 Ωcm^2, and the interfacial polarization resistances are 2.41, 1.06 and 0.57 Ωcm^2 at 600, 650 and 700 °C, respectively, suggesting that the reductions of polarization resistance of cell are the main contributions of the decrease in the cell resistance. The total resistances of cells are 3.30, 1.73 and 1.09 Ωcm^2 at 600, 650 and 700 °C, respectively, much larger than ASRs calculated from the *I–V* curves as discussed above, especially the ones in SOEC mode.

To investigate the electrode performance under operation conditions in details, the impedance spectra of the cells were then measured at 700 °C in SOFC mode (discharging at 0.7 V) and SOEC mode (electrolysis at 1.3 V) with the steam partial pressure of 50%, as shown in Fig. 3(a) and (b). The total cell resistances are determined to be 0.94 Ωcm^2 in SOFC mode and 0.74 Ωcm^2 in SOEC mode, respectively, which are more close to their resistances simulated from *I–V* curves than that measured under OCV conditions. It should be noted that the bulk resistances of cells in both operating modes are about 0.52 Ωcm^2, which is independent of the potential load and almost the same with that calculated under OCV conditions. However, the interfacial polarization resistances differ in the two operating modes, being about 0.52 Ωcm^2 in SOFC mode and 0.22 Ωcm^2 in SOEC mode, which are both lower than that measured under OCV conditions. According to Fig. 3, it can be seen that each spectrum is composed of two depressed arcs, a high frequency arc and a low frequency arc. An equivalent circuit comprises of two *RQ* elements and one *R* in series, $R_{bulk}(R_HQ_H)(R_LQ_L)$, were proposed to solve these spectra. Based on these results, the high frequency resistances (R_H) and low frequency resistances (R_L) are calculated to be 0.07 and 0.36 Ωcm^2 in SOFC mode, and 0.15 and 0.07 Ωcm^2 in SOEC mode, respectively.

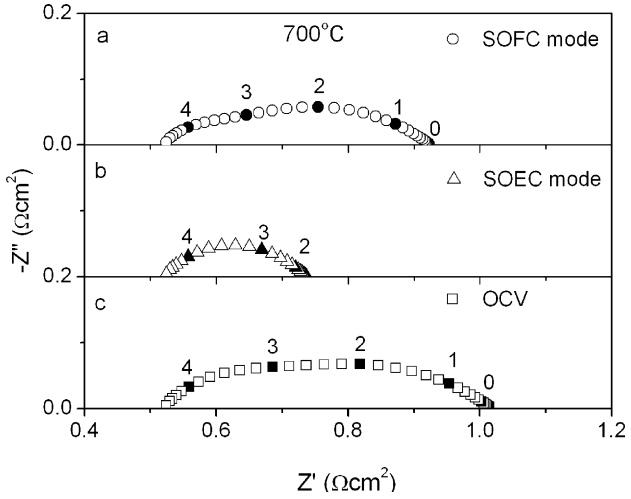

Fig. 3. Impedance spectra of the R-SOFCs with 50%H_2O–air and H_2 as reacting gas measured (a) in SOFC mode (0.7 V), (b) in SOEC mode (1.3 V), and (c) in open circuit mode. Numbers 0–4 in spectra denotes the frequency order.

With the comparison of the resolved resistances in SOFC mode and SOEC mode, it can be seen that R_H in SOEC mode is almost twice of that in SOFC mode, but R_L in SOEC mode is almost reduced to zero. Assuming that (1) there is no material components transfer or microstructure change during the spectra measurement, since the measurements occur at the same time with the input of bias potential; (2) the generation/exhaustion of O_2 at oxygen electrodes during cell operation has few effect on the electrode performance, since the oxygen generation or consumption rates are 0.22 and 0.73 ml min^{-1} for SOFC and SOEC modes, respectively, only 1.0% and 3.6%; (3) the proton diffusion in the anode is not the rate-limiting process, which has been previously proved by the literature [20], the difference in the measured spectra resulted only from the change of the rate-limiting process in the cathode reactions. Earlier we have investigated the elementary steps of SSC–BCS composite electrode with the proton electrolyte using symmetric cells, as shown in Step 1–Step 8, and found that the migration of protons to three phase boundaries (Step 5, corresponding to the high frequency arc) and the surface diffusion of O_{ad}^+ (Step 3 related to the low frequency arc) were the rate-limiting process in SOFC mode under wet conditions [21]. In present case since the low frequency arc disappears in SOEC mode, the surface diffusion of O_{ad}^- might not be the rate-limiting process.

Step1 : $O_{2(g)} \rightarrow 2O_{ad}$

Step2 : $O_{ad} + e^- \rightarrow O_{ad}^-$

Step3 : $O_{ad}^- \rightarrow O_{TPB}^-$

Step4 : $O_{TPB}^- + e^- \rightarrow O_{TPB}^{2-}$

Step5 : $H_{electrolyte}^+ \rightarrow H_{TPB}^+$

Step6 : $H_{TPB}^+ + O_{TPB}^{2-} \rightarrow OH_{TPB}^-$

Step7 : $H_{TPB}^+ + OH_{TPB}^- \rightarrow H_2O_{TPB}$

Step8 : $H_2O_{TPB} \rightarrow H_2O(g)$

To clarify the difference in impedance spectra under two operating modes, the anodic elementary steps of SOEC reactions are proposed as Step I–Step IX:

StepI : $H_2O(g) \rightarrow H_2O_{ad}$

StepII : $H_2O_{ad} \rightarrow OH_{ad}^- + H_{ad}^+$

StepIII : $OH_{(ad)}^- \rightarrow O_{ad}^{2-} + H_{ad}^+$

StepIV : $O_{ad}^{2-} - e \rightarrow O_{ad}^-$

StepV : $O_{ad}^- - e \rightarrow O_{ad}$

StepVI : $2O_{ad} \rightarrow O_2(ad)$

StepVII : $O_2(ad) \rightarrow O_2$

StepVIII : $H_{ad}^+ \rightarrow H_{TPB}^+$

StepIX : $H_{TPB}^+ \rightarrow H_{electrolyte}^+$

where Step I–Step III describe the surface dissociative adsorption of water to O^{2-} and protons; Step IV–Step VII illustrate the formation and desorption of O_2 along with the charge transfer; Step

VIII and Step IX depict the proton migration to triple phase boundaries (TPBs). Comparing the elementary steps in SOFC and SOEC modes, one can clearly see that the surface diffusion of O_{ad}^- (low frequency arc) is not the elementary step in SOEC mode, since the O^{2-} and O^- could readily accept electrons on the right surface of SSC and consequently there was no need for them to transfer to the TPBs. This is in good accordance with the impedance spectra measurements. It should also be noted that the transfer of protons involve two steps in SOEC mode: (1) the protons decomposed from water (H_{ad}^+) transferring to the triple phase boundaries; (2) the protons at TPBs (H_{TPB}^+) transferring to the electrolyte, as shown in Steps VIII and IX. While in SOFC mode, the protons only transfer from electrolyte to the TPBs (Step 5). This might be the right answer for the significant increase of the high frequency resistances (R_H) in SOEC mode compared with that in SOFC mode.

It is also noteworthy that the impedance spectrum under OCV conditions has different shapes with those both in SOFC mode and SOEC mode, as shown in Fig. 3(c). The simulated R_H under OCV conditions is 0.13 Ωcm^2, close to R_H in SOEC mode, while R_L under open circuit conditions is 0.39 Ωcm^2 which is close to R_L in SOFC mode. It seems that the spectra of cells under open circuit conditions are the combination of high frequency arc in SOEC mode and low frequency arc in SOFC mode. That might be due to the 'competition' result of elementary reactions in SOFC and SOEC modes, since all of them exist under open circuit conditions with similar peak frequency corresponding to high and low frequency arcs, respectively. This also suggests that the limiting reactions corresponding to the spectra for R-SOFCs-H in OCV conditions are the decomposed protons (H_{ad}^+) transferring to the electrolyte (SOEC mode, the high frequency arc) and the surface diffusion of O_{ad}^- to TPBs (SOFC mode, the low frequency arc).

3.2. Electrochemical performance of the cells with different steam partial pressures

The performance of the cells was also characterized with various steam concentrations at the oxygen electrode, as shown in Fig. 4. The OCV decreased with the increase of the steam concentration, which is about 1.01, 1.00, 0.95, 0.88 V under the steam partial pressureS of 20%, 30%, 50%, 70%, respectively (measured at 700 °C). The discharging performance of the cell also decreased with the increase of the steam concentration, and the maxima power densities are 289, 254, 234 and 208 mW cm^{-2} with the steam partial pressure of 20%, 30%, 50%, and 70%, respectively. While the electrolysis performance of the cell increased with steam concentration. At

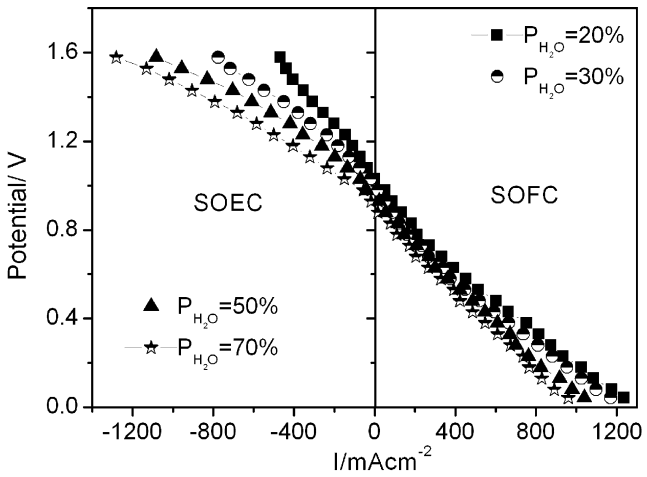

Fig. 4. Voltage–current density curves of the R-SOFCs tested at 700 °C with various H_2O partial pressures in oxygen electrode.

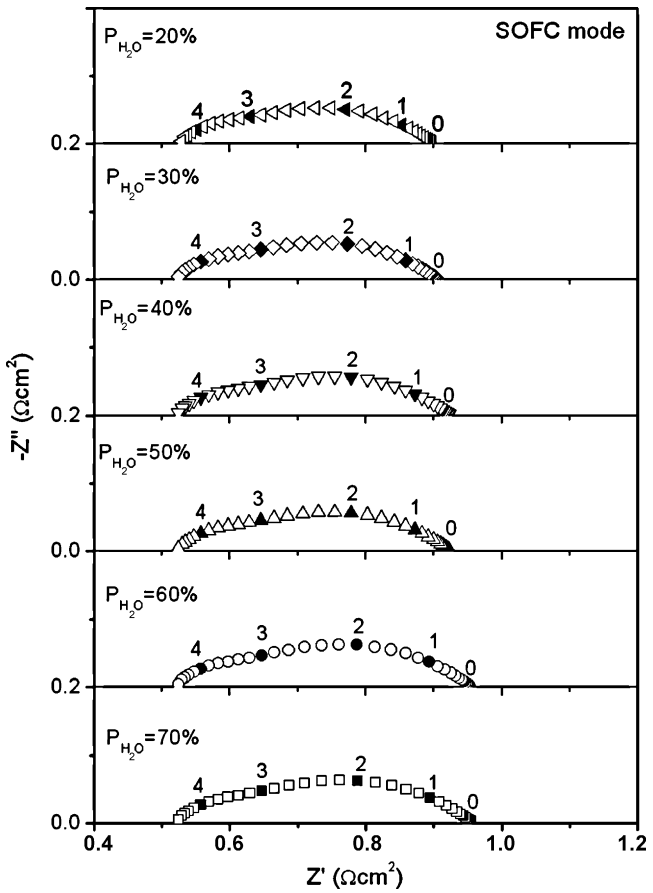

Fig. 5. Impedance spectra of the R-SOFCs measured at 700 °C in SOFC mode (0.7 V) with various steam partial pressures in oxygen electrode. Numbers 0–4 in spectra denotes the order of frequency.

700 °C and 1.5 V, the electrolysis current densities are −404, −623, −830, −1010 mA cm^{-2} with the steam partial pressure of 20%, 30%, 50%, 70%, respectively.

The impedance spectra of the cells under SOFC, SOEC and OCV modes were next investigated with various steam partial pressures at the oxygen electrode measured at 700 °C, as shown in Figs. 5–7. The bulk resistances in all the three modes remain about 0.52 Ωcm^2, almost constant with the water partial pressure. While the dependence of polarization resistances on steam partial pressure are quite different in these three modes. The polarization resistances in SOFC mode increased slightly with the steam partial pressure, about 0.38, 0.38, 0.40, 0.43, 0.44, 0.45 Ωcm^2 with steam partial pressure of 20%, 30% 40%, 50%, 60% and 70%, respectively. While the polarization resistances in SOEC mode decrease largely first with the increase of steam partial pressure, and then keep stable when the steam partial pressures are larger than 50%. The polarization resistances in SOEC mode are about 0.44, 0.41, 0.35, 0.22, 0.21 and 0.20 Ωcm^2 with the steam partial pressures of 20%, 30% 40%, 50%, 60% and 70%, respectively.

These impedance spectra were also resolved by an equivalent circuit $R_{electrolyte}(R_HQ_H)(R_LQ_L)$, and the results are shown in Table 1. It can be seen that the high frequency resistances of cells in both SOFC mode and SOEC mode remain unchanged with the steam partial pressure while the low frequency resistance increased in SOFC mode but decreased in SOEC mode instead. This is quite different with their performance in the symmetric cells [21], of which the dependence of high frequency resistances on steam partial pressure can be expressed as $R_H \prec P_{H_2O}^{-1/2}$ whereas the low frequency resistance kept almost unchanged. The different dependences of

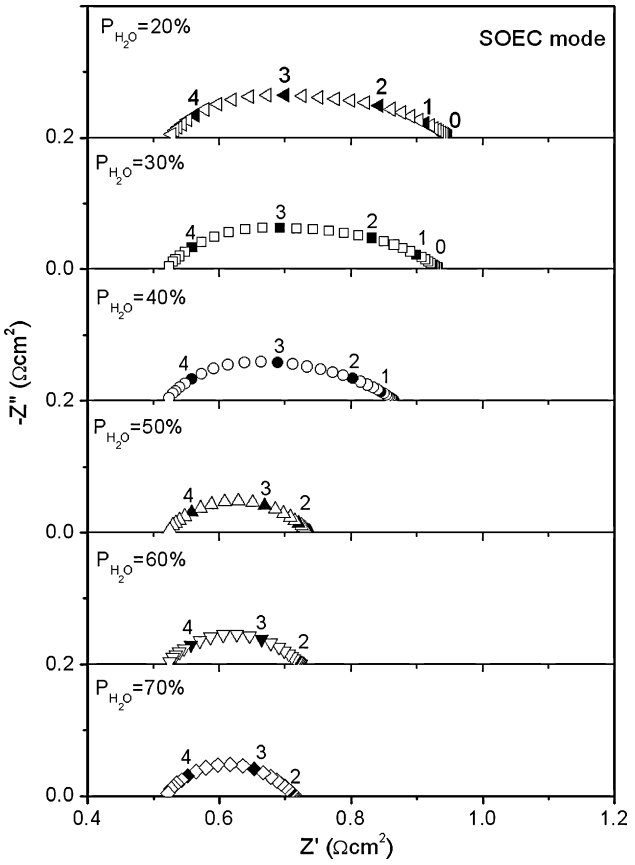

Fig. 6. Impedance spectra of the R-SOFCs measured at 700 °C in SOEC mode (1.3 V) with various steam partial pressures in oxygen electrode.

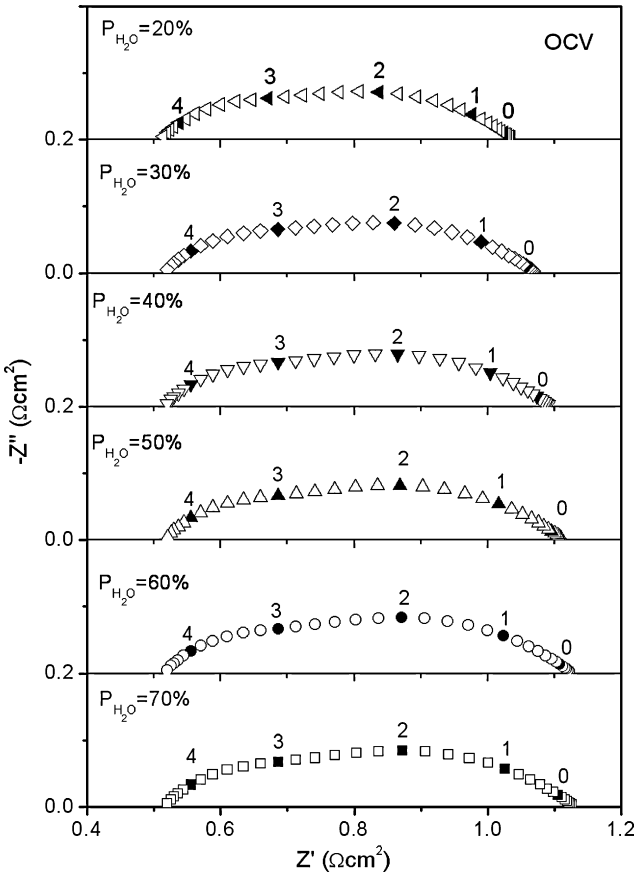

Fig. 7. Impedance spectra of the R-SOFCs measured at 700 °C in open circuit conditions with various steam partial pressures in oxygen electrode.

R_H on steam partial pressure in symmetric cells and operating cells mainly result from the dependence of proton concentration on partial pressure. In the symmetric cells, the protons are generated by the incorporation of water within lattice, and their concentrations keep in balance with the low steam partial pressure, resulting in the migration of protons greatly dependant on the steam partial pressure. While in the operating cells, the protons concentration are affected not only by the steam partial pressure, but also by the pressure of H_2 at the hydrogen electrodes, leading to the imbalance between proton concentrations and steam partial pressure and thus the independence of proton transfers on steam partial pressure. The decrease/increase of the low frequency resistances in SOEC/SOFC mode with the steam partial pressure might be due to the concentration polarization resistance, since the obvious decrease in SOEC mode occurs at the steam partial pressure over 50%. Detailed investigations about the effect of steam partial pressure on polarization resistances are yet to be done.

The impedance spectra under OCV conditions were also resolved and the data are summarized in Table 1 as well. The high frequency resistances are still close to R_H in SOEC mode, whereas the low frequency resistances are close to R_L in SOFC mode instead. This result is in accordance with our foregoing observation, as shown in Fig. 8.

Table 1
Bulk resistances (R_b), high frequency resistances (R_H) and low frequency resistances (R_L) simulated from impedance spectra under various potentials and stream partial pressure.

Bias potential	Stream partial pressure	R_b (Ωcm^2)	R_H (Ωcm^2)	R_L (Ωcm^2)
0 V	20%	0.52	0.13	0.33
	50%	0.51	0.13	0.39
	70%	0.52	0.14	0.41
−0.3 V	20%	0.52	0.07	0.32
	50%	0.51	0.07	0.36
	70%	0.52	0.07	0.38
+0.3 V	20%	0.52	0.16	0.28
	50%	0.52	0.15	0.07
	70%	0.52	0.15	0.05

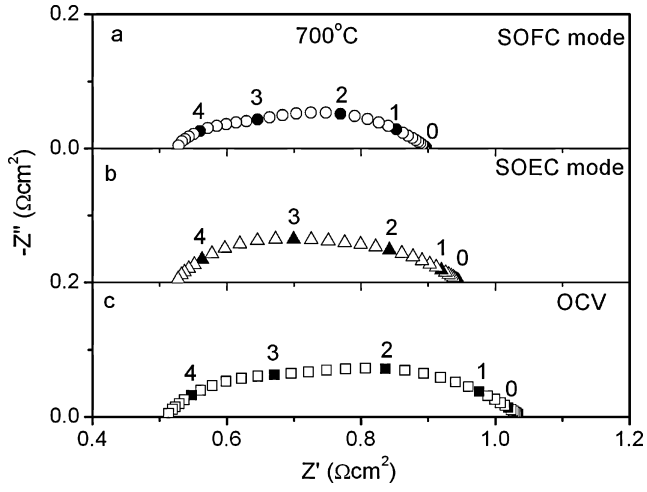

Fig. 8. Impedance spectra of the R-SOFCs measured at 700 °C (a) in SOFC mode (0.7 V), (b) in SOEC mode (1.3 V), and (c) under open circuit conditions with 20%H_2O–air and H_2 input into oxygen electrode and hydrogen electrode, respectively.

Since the high frequency resistances of SOEC barely change with the increase of the steam partial pressure, while the low frequency resistances of SOFC increased with such an increase, the polarization resistances in OCV conditions reasonably increased with the increase of the steam partial pressures, as clearly demonstrated in Fig. 7.

4. Conclusions

Reversible solid oxide fuel cells (R-SOFCs) with structure of Ni-BCZY || $BaCe_{0.5}Zr_{0.3}Y_{0.2}O_{3-\delta}$ (BCZY) || SSC–BCZY were fabricated by dry-pressing process. At 700 °C, with 50% H_2O–air and H_2 introduced into oxygen electrode and hydrogen electrode, respectively, the charging current is 251 mA cm^{-2} at 0.7 V and maximum powder density reaches 234 mW cm^{-2} at 0.48 V. The electrolysis current density achieves −830 mA cm^{-2} at 1.5 V under the same testing conditions, about one order of magnitude larger than previous report due to the reduce in electrolyte thickness.

The impedance spectra study suggests that there are two arcs, a high frequency arc and a low frequency arc, in the spectra tested under open circuit conditions, which changed differently with the bias potential. In SOFC mode, the high frequency arc decrease to half of that in OCV conditions, while the low frequency remained unchanged. In SOEC mode, the high frequency arc hardly changed compared with that in OCV conditions, while the low frequency arc almost disappeared. High frequency resistances (R_H) and low frequency resistances (R_L) are simulated as 0.07 and 0.36 Ωcm^2 in SOFC mode, 0.15 and 0.07 Ωcm^2 in SOEC mode, and 0.13 and 0.39 Ωcm^2 under OCV mode, respectively. The elementary steps for steam electrolysis with proton conducting electrolyte were proposed to account for this phenomenon. The results suggest that the surface diffusion of O_{ad}^-, corresponding to low frequency arc, is not the elementary step for SOEC reaction, which was in good accordance with the very low frequency resistance in spectra investigation. It was also suggested that the transfer of protons involves two steps in SOEC mode: the protons decomposed from water (H_{ad}^+) transferring to the triple phase boundaries and the protons at TPBs (H_{TPB}^+) transferring to the electrolyte, which might be the right reason for the large R_H in SOEC.

Acknowledgements

This work was supported by the Natural Science Foundation of China (50602043, 50730002, 20801052), and by the National High Technology Research and Development Program of China (2007AA05Z157 and 2007AA05Z151).

References

[1] A.B. Stambouli, E. Traversa, Renewable & Sustainable Energy Reviews 6 (2002) 433–455.
[2] K. Eguchi, T. Hatagishi, H. Arai, 10th International Conference on Solid State Ionics (SSI-10), Singapore, Singapore, 1995, pp. 1245–1249.
[3] J.S. Herring, J.E. O'Brien, C.M. Stoots, G.L. Hawkes, J.J. Hartvigsen, M. Shahnam, International Journal of Hydrogen Energy 32 (2007) 440–450.
[4] M.D. Liang, B. Yu, M.F. Wen, J. Chen, J.M. Xu, Y.C. Zhai, Journal of Power Sources 190 (2009) 341–345.
[5] M.A. Laguna-Bercero, S.J. Skinner, J.A. Kilner, Journal of Power Sources 192 (2009) 126–131.
[6] J.E. O'Brien, C.M. Stoots, J.S. Herring, P.A. Lessing, J.J. Hartvigsen, S. Elangovan, Journal of Fuel Cell Science and Technology 2 (2005) 156–163.
[7] J. Schefold, A. Brisse, M. Zahid, Journal of the Electrochemical Society 156 (2009) B897–B904.
[8] Y. Shin, W. Park, J Chang, J. Park, 2nd European Hydrogen Energy Conference, Zaragoza, Spain, 2005, pp. 1486–1491.
[9] M. Ni, M.K.H. Leung, D.Y.C. Leung, International Journal of Hydrogen Energy 33 (2008) 2337–2354.
[10] A. Hauch, S.D. Ebbesen, S.H. Jensen, M. Mogensen, Journal Of Materials Chemistry 18 (2008) 2331–2340.
[11] G. Schiller, A. Ansar, M. Lang, O. Patz, Journal of Applied Electrochemistry 39 (2009) 293–301.
[12] M. Ni, M.K.H. Leung, D.Y.C. Leung, International Journal of Hydrogen Energy 33 (2008) 4040–4047.
[13] M. Ni, M.K.H. Leung, D.Y. Leung, Journal of Power Sources 177 (2008) 369–375.
[14] H. Iwahara, T. Esaka, H. Uchida, N. Maeda, Solid State Ionics 3–4 (1981) 359–363.
[15] T. Kobayashi, K. Abe, Y. Ukyo, H. Matsumoto, Solid State Ionics 138 (2001) 243–251.
[16] P.A. Stuart, T. Unno, J.A. Kilner, S.J. Skinner, Solid State Ionics 179 (2008) 1120–1124.
[17] T. Sakai, S. Matsushita, H. Matsumoto, S. Okada, S. Hashimoto, T. Ishihara, International Journal of Hydrogen Energy 34 (2009) 56–63.
[18] R.R. Peng, Y. Wu, L.Z. Yang, Z.Q. Mao, Solid State Ionics 177 (2006) 389–393.
[19] W. Zhu, C.R. Xia, J. Fan, R.R. Peng, G.Y. Meng, Journal of Power Sources 160 (2006) 897–902.
[20] T.Z. Wu, Y.Q. Zhao, R.R. Peng, C.R. Xia, Electrochimica Acta 54 (2009) 4888–4892.
[21] F. He, T.Z. Wu, R.R. Peng, C.R. Xia, Journal of Power Sources 194 (2009) 263–268.